

c-MYC Generates Repair Errors via Increased Transcription of Alternative-NHEJ Factors, LIG3 and PARP1, in Tyrosine Kinase-Activated Leukemias

Nidal Muvarak^{1,2}, Shannon Kelley^{3,4}, Carine Robert^{1,2}, Maria R. Baer^{2,5}, Danilo Perrotti^{2,5,6}, Carlo Gambacorti-Passerini⁷, Curt Civin^{3,4}, Kara Scheibner^{3,4}, and Feyruz V. Rassool^{1,2}

Abstract

Leukemias expressing the constitutively activated tyrosine kinases (TK) BCR-ABL1 and FLT3/ITD activate signaling pathways that increase genomic instability through generation of reactive oxygen species (ROS), DNA double-strand breaks (DSB), and error-prone repair. The nonhomologous end-joining (NHEJ) pathway is a major pathway for DSB repair and is highly aberrant in TK-activated leukemias; an alternative form of NHEJ (ALT-NHEJ) predominates, evidenced by increased expression of DNA ligase III α (LIG3) and PARP1, increased frequency of large genomic deletions, and repair using DNA sequence microhomologies. This study, for the first time, demonstrates that the TK target c-MYC plays a role in transcriptional activation and subsequent expression of LIG3 and PARP1 and contributes to the increased error-prone repair observed in TK-activated leu-

kemias. c-MYC negatively regulates microRNAs miR-150 and miR-22, which demonstrate an inverse correlation with LIG3 and PARP1 expression in primary and cultured leukemia cells and chronic myelogenous leukemia human patient samples. Notably, inhibition of c-MYC and overexpression of miR-150 and -22 decreases ALT-NHEJ activity. Thus, BCR-ABL1 or FLT3/ITD induces c-MYC expression, leading to genomic instability via augmented expression of ALT-NHEJ repair factors that generate repair errors.

Implications: In the context of TK-activated leukemias, c-MYC contributes to aberrant DNA repair through downstream targets LIG3 and PARP1, which represent viable and attractive therapeutic targets. *Mol Cancer Res*; 13(4); 699–712. ©2015 AACR.

Introduction

Constitutively activated tyrosine kinases (TK) BCR-ABL1 and FLT3/ITD generate increased levels of reactive oxygen species (ROS), DNA damage including double-strand breaks (DSB) and abnormal repair that is highly error-prone. Together, these features result in acquisition of genomic alterations which have the potential to drive disease progression and resistance to therapy (1, 2). DSBs are repaired by 2 pathways, homologous recombination (HR) and nonhomologous end-joining (NHEJ; refs. 3–5).

The classic NHEJ (c-NHEJ) pathway frequently causes small alterations in DNA sequences around the break site but rarely joins previously unlinked DNA ends (6). However, there is an alternative (ALT) version of NHEJ that results in larger deletions and chromosomal translocations where DNA ends are joined at regions of DNA sequence microhomology (6, 7). Notably, ALT-NHEJ activity is increased when the c-NHEJ pathway is down-regulated (6, 7). Expression of both BCR-ABL1 and FLT3/ITD significantly alters the expression of key DSB repair components at both the mRNA and protein levels (8) and increases the frequency of repair errors (9–12). These cells also demonstrate increased in ALT-NHEJ activity characterized by large DNA deletions and repair using DNA sequence microhomologies (8, 13, 14). Notably, treatment of BCR-ABL1- and FLT3/ITD-positive cells with TK inhibitors (TKI) leads to decreased expression of ALT-NHEJ components LIG3 and PARP1 (8, 13, 14) and decreased DSB repair errors, indicating that altered DNA repair is due to one or more effectors of these signaling pathways (12). However, the mechanisms responsible for this repair dysregulation were unknown.

There are several routes through which mammalian cells regulate gene expression, with transcriptional regulation being the most common mechanism. Both FLT3/ITD- and BCR-ABL1-activated leukemias exhibit induction of the oncogenic transcription factor c-MYC (15, 16). In turn, many downstream targets of c-MYC are transcriptionally activated, and this increased signaling may result in enhanced survival and genomic instability (17). In fact, c-MYC interacts with and regulates the promoters of DSB

¹Department of Radiation Oncology, University of Maryland School of Medicine, Baltimore, Maryland. ²Marlene and Stewart Greenebaum Cancer Center, University of Maryland School of Medicine, Baltimore, Maryland. ³Department of Pediatrics, University of Maryland School of Medicine, Baltimore, Maryland. ⁴The Center for Stem Cell Biology and Regenerative Medicine, University of Maryland School of Medicine, Baltimore, Maryland. ⁵Department of Medicine, University of Maryland School of Medicine, Baltimore, Maryland. ⁶Department of Haematology, Hammersmith Hospital, Imperial College London, London, United Kingdom. ⁷University of Milano-Bicocca Monza, Italy.

Note: Supplementary data for this article are available at Molecular Cancer Research Online (<http://mcr.aacrjournals.org/>).

Corresponding Author: Feyruz V. Rassool, Department of Radiation Oncology, 655 West Baltimore Street, Baltimore, MD 21201. Phone: 410-706-5337; Fax: 410-706-6666; E-mail: FRassool@som.umaryland.edu

doi: 10.1158/1541-7786.MCR-14-0422

©2015 American Association for Cancer Research.

repair genes in several cancer cell lines (18). While the functional significance of this regulation remains unclear, these studies suggest that c-MYC might contribute to the DNA repair abnormalities observed in acute myeloid leukemia (AML) and chronic myelogenous leukemia (CML) cells with BCR-ABL1 and FLT3/ITD mutations. In addition, c-MYC has been shown to negatively regulate specific miRNAs, with c-MYC induction leading to repression of multiple miRNAs and miRNA clusters (19).

In this study, we investigated the role of c-MYC in error-prone repair through increased expression of ALT-NHEJ factors LIG3 and PARP1 in cell lines and primary myeloid malignancies and demonstrated that both c-MYC and c-MYC-regulated miRNAs, miR-150 and miR-22, contribute to increased levels of LIG3 and PARP1 expression, and consequently, ALT-NHEJ activity.

Materials and Methods

Patient samples

Frozen mononuclear cells (MNC) from bone marrow and peripheral blood samples were obtained from patients with CML [chronic phase (CP), $n = 15$; accelerated phase (AP), $n = 1$; blast crisis (BC), $n = 14$] at the Marlene and Stewart Greenebaum Cancer Center and at the University of Milano-Bicocca on protocols approved by the Institutional Review Board. Bone marrow MNC from healthy donors (HD; Lonza) were used as controls for the patient samples.

Cell lines and culture

The murine myeloid precursor cell lines 32Dcl3 and 32D-FLT3/ITD (kindly provided by Dr. Donald Small, Johns Hopkins University, Baltimore, MD), the human megakaryocytic cell lines MO7e and MO7e-BCR-ABL1 (kindly provided by Dr. Richard van Etten, Tufts University, Boston, MA), the human AML cell line MOLM14 (expressing FLT3/ITD), the human leukemia cell line REH (expressing wild-type FLT3), and the human CML cell line K562 (established from a patient in blast crisis; ref. 20) were grown as previously described (11, 14). 293T human embryonic kidney cells were grown in DMEM supplemented with 10% FBS.

Plasmids

The c-MYC expression vectors pBABEpuro-myc-ER (plasmid 19128) and pcDNA3-cmyc (plasmid 16011) were obtained from Addgene and described in Ricci and colleagues (21). The luciferase expression vector pGL4.10 was obtained from Promega. To construct the LIG3 promoter-reporter construct (pGL4.10-LIG3p), we cloned the LIG3 promoter from BAC clone 3143J8 (Invitrogen) using forward-AACCCTAACACCTCCTCCTCTCT and reverse-TGATCAAGGCTCCCTGAGTCCCA primers (IDT Technologies). The cloned promoter was digested with *NheI* and *EcoRV* restriction enzymes (New England Biolabs) and inserted into a digested pGL4.10 vector using a T4 ligase kit (Promega) according to the manufacturer's instructions. The PARP1 promoter-reporter construct was obtained from Switch Gear Genomics. The carbamoyl-phosphate synthetase 2 (*CAD*) promoter was cloned from gDNA isolated from normal human bone marrow (Lonza) using forward-TGGGAGCCACCACTCTAT and reverse-CGCATCACAGAGTGGGATAA primers and then digested with *SacI* restriction enzyme and cloned into pGL4.10 using T4 ligase kit. For site-directed mutagenesis of the c-MYC binding sites within the constructs above, we used the Q5 Site-Directed Mutagenesis Kit (New England Biolabs) according to the manufacturer's instructions.

All promoter-reporter reporter constructs were sequenced to confirm correct orientation and sequence of promoters, as well as success of site-directed mutagenesis. A GFP-expressing plasmid, pmaxGFP (Lonza), was used throughout the study to control for transfection efficiency. pEF1alpha-DsRed-Express 2 vector (Clontech) was used as a transfection efficiency control for experiments using pEGFP-Pem1-Ad2 vector (kindly provided by Dr. Vera Gorbunova, University of Rochester, NY).

Western blotting

Western blot analysis was performed as previously described (14). c-MYC and Ku70 (Santa Cruz Biotechnology) antibodies were used at 1:500 and 1:1,000, respectively. Anti-LIG3 (clone 7, BD Biosciences) and anti-PARP1 (Cell Signaling Technologies) were used at 1:3000. Anti-LIG4 (GeneTex) was used at 1:1,000. Anti-GRB2 (Cell Signaling Technology) was used at 1:1,000. Anti-actin antibody (Sigma) was used as a loading control at 1:10,000. Secondary antibodies conjugated to horseradish peroxidase (HRP; KPL) were added at a 1:10,000 dilution. Signal was detected using ECL (GE Healthcare). Bands were quantified with ImageQuant software (Bio-Rad).

Quantitative PCR

RNA isolation for real-time PCR of c-MYC, LIG3, and PARP1 transcripts was performed using the RNAspin mini-kit (GE Healthcare). Quantitect Primers (Qiagen) were used for each target, with *GAPDH* as housekeeping gene. Power SYBR Green RT-PCR Mastermix (Applied Biosystems) was used for reactions carried out in triplicates using a Mastercycler ep (Eppendorf). Relative quantification was determined using Eppendorf *realplex* software according to the $\Delta\Delta C_T$ method. For ChIP-qPCR, we used HotStart-IT SYBR Green qPCR 2X Mastermix (Affymetrix) per the manufacturer's instructions.

Nanosting microRNA analysis

Paired CML-CP ($n = 5$), CML-BC ($n = 5$), and from HD ($n = 3$) MNCs were processed using Ficoll-Paque plus (GE Healthcare Life Sciences). Total RNA was extracted with TRIzol (Invitrogen) per the manufacturer's instructions, and 100 ng per sample was used to assess differences in miRNA expression using multiplexed NanoString enzyme-independent probe-based quantification system that allows digital counting of individual miRNA molecules (nCounter; NanoString Technologies), as previously described (22). NanoString assays were performed at the Ohio State University Comprehensive Cancer Center Microarray Facility (Columbus, OH). Heatmap analysis was performed using z-score.

siRNA knockdown

Cells (2×10^6 , 0.5×10^6 per mL) were washed in Opti-MEM medium (Invitrogen) and transfected with SMARTpool siRNA (Thermo Scientific Dharmacon), or single siRNA (Cell Signaling Technologies) using the Amaxa Nucleofection System (Lonza) as previously described (14).

MiRNAs

Total RNA was isolated using miRNeasy kit (Qiagen) per the manufacturer's instructions. Levels of miRNAs were determined by qPCR using a TaqMan qRT-PCR kit (Life Technologies), with U18 serving as the housekeeping miRNA. miRNA expression and microarray analyses were carried out as previously described (23).

For miRNA overexpression experiments, K562, MO7e-BCR/ABL1, and MOLM-14 cells were transfected with 50 nmol/L miR-34a, -22, -150, or a combination of miR-22 and -150 (Thermo Scientific-Dharmacon) and harvested for Western blotting and NHEJ repair analyses at 24, 48, or 72 hours posttransfection.

Chromatin immunoprecipitation

Chromatin immunoprecipitation (ChIP) was performed according to Luoto and colleagues (18), with the following modifications. Lysates were sonicated on ice 10 times using a Branson 450 Sonifier for 10 seconds each time, at 40% output control and 2.5 duty cycle, with 30-second refractory periods between sonications. ChIP products were purified using a Qiaquick kit (Qiagen) followed by qPCR using the following primer sets:

LIG3(forward) 5'-AACTACTCCCAAACATCACAGG-3'
 LIG3(reverse) 5'-CTTTAAATCCGGGTCTAGAGC-3'
 PARP1(forward) 5'-GGTCTCAAACCTCTGCTACAA-3'
 PARP1(reverse) 5'-AGGACACACTTAAGAGTTTGGG-3'
 CAD(forward) 5'-TAGCCACGTGGACCCACT-3'
 CAD(reverse) 5'-TACGGAGAAGCGGGAAGGA-3'
 Ch22(forward) 5'-GGATGACAGGCATGAGGAATTA-3'
 Ch22(reverse) 5'-TGCTGCTTACTTGGGATATGAG-3'

Luciferase assays

32D-FLT3/ITD and MO7e-BCR-ABL1 cells were transfected with control or c-MYC-targeting siRNA as described above. Transfected cells were incubated for 48 hours and then harvested for transfection with luciferase constructs pGL4.10 (promoterless control, Promega) or pGL4.10-LIG3p and pGL4.10-PARP1p (luciferase vectors containing LIG3 and PARP1 promoters, respectively). Transfection efficiency was determined by cotransfection with pRL-TK vector (Promega) containing HSV thymidine kinase promoter. Measurement of luciferase activity was performed with Dual Luciferase Reporter Assay System (Promega) using an HT Synergy plate reader (Bio-TEK).

In vivo NHEJ assay

The *in vivo* NHEJ assay was performed as previously described (14). Briefly, 0.2 µg of linearized pUC18 plasmid was transfected into 2×10^6 cells 48 hours posttransfection with siRNA against c-MYC or miR-22/150 combination, respectively. Repaired plasmid clones were sequenced at the repair junction, and sequences were analyzed using BioEdit sequence alignment editor (<http://www.mbio.ncsu.edu/bioedit/bioedit.html>). Three independent c-MYC knockdown or miRNA overexpression experiments, followed by 3 independent *in vivo* NHEJ assays were performed to confirm results. To determine the relative end-joining efficiency after siRNA knockdown, we used the GFP-based end-joining assay described by Fattah and colleagues (Fattah, 2010, #11559). Briefly, cells were transfected with siRNA for 48 hours, followed by transfection with *Hind*III-linearized pEGFP-Pem1-Ad2. Twenty-four hours later, the cells were analyzed by flow cytometry for GFP. For this assay, a DsRed expression plasmid (pEF1alpha-DsRed-Express 2) was used to normalize for any variations in transfection efficiency.

Statistical analysis

Statistical analysis comparing experimental and control groups was performed using the Student *t* test and *z*-test (for differences in frequencies of microhomology-mediated repair

and proportions of patient samples). The correlation coefficient (Pearson *R*) was used to determine positive or negative correlations.

Results

c-MYC expression is elevated in TK-activated myeloid leukemias and correlates with LIG3 and PARP1 expression levels

Our previous studies showed that TK-activated leukemias had increased steady-state levels of PARP1 and LIG3 mRNA and protein (12), suggesting that they are transcriptionally regulated. Following database analysis (using MatInspector from Genomatix) and TF Search (Parallel Application TRC Laboratory) of promoter regions of these genes, c-MYC binding sites were revealed and thus c-MYC was investigated as a candidate in transcriptional regulation of these genes.

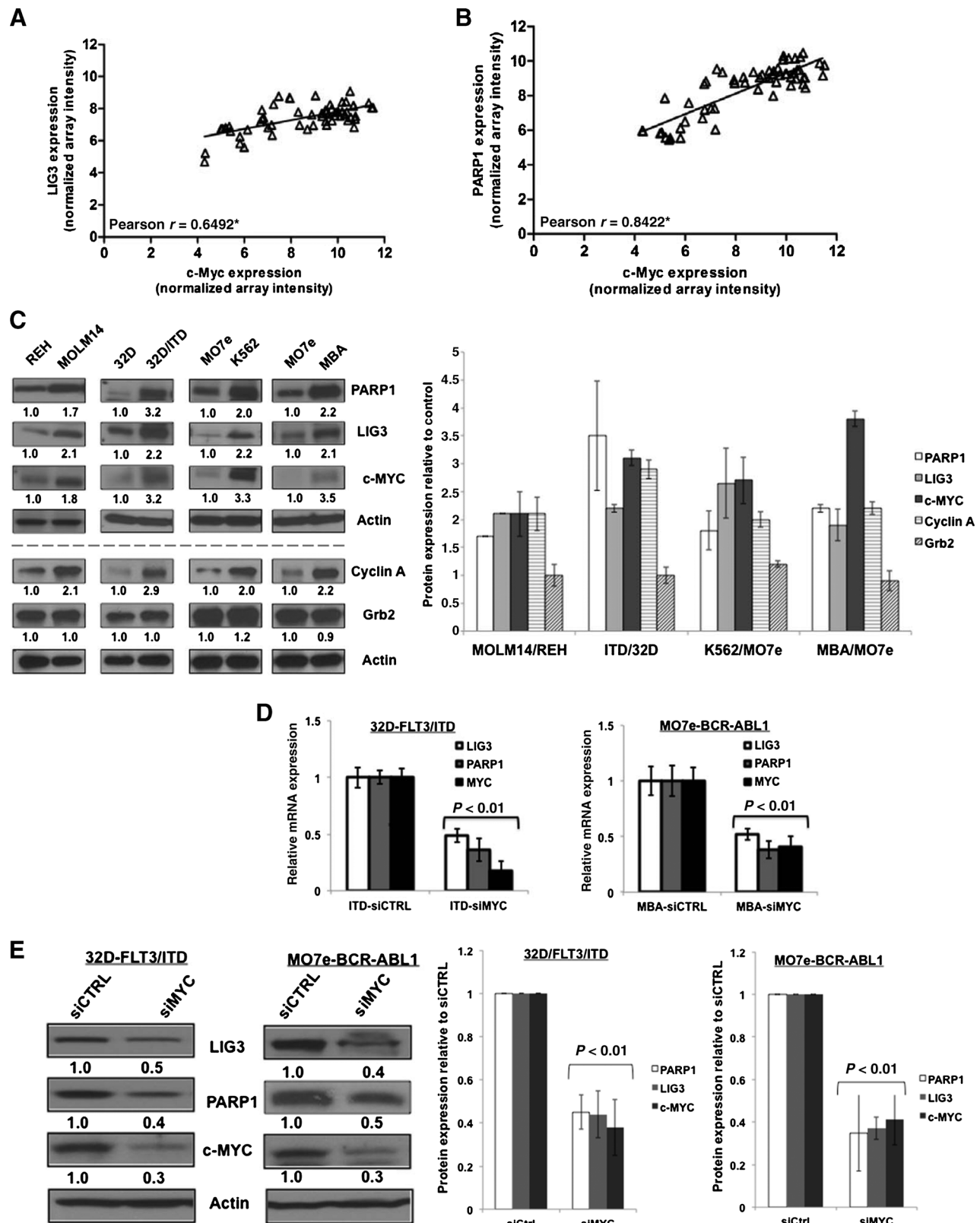
To determine whether c-MYC plays a role in regulating expression of LIG3 and PARP1, we initially examined microarray data for multiple myeloid leukemia cell lines and primary cells to correlate mRNA expression levels of c-MYC with either LIG3 and PARP1 mRNA expression levels. Analysis of AML cell lines (HL60, Kasumi1, KG1a, ML2, Mo7e, and U937), the BCR-ABL1+ CML cell line in blast crisis K562 and primary AML patient samples ($n = 18$; Supplementary Table S1) revealed that endogenous levels of c-MYC showed a significant positive correlation, with levels of LIG3 (Pearson $R = 0.6492$; Fig. 1A) and PARP1 (Pearson $R = 0.8422$; Fig. 1B).

Given the strong correlation of c-MYC mRNA levels with LIG3 and PARP1 mRNA levels in AML, we hypothesized that increased c-MYC expression may augment expression of LIG3 and PARP1 in TK-activated leukemias, in which c-MYC is known to be expressed at high levels (15, 16). We first assessed protein levels of c-MYC, LIG3, and PARP1 in cell extracts from hematopoietic cell lines that stably express BCR-ABL1 (MO7e-BCR-ABL1) or FLT3/ITD (32D-FLT3/ITD) and their respective parental controls (MO7e and 32Dcl3). In addition, leukemia cell lines endogenous protein levels were compared in FLT3/ITD-positive MOLM14 versus wild-type FLT3 REH and BCR-ABL1-positive K562 versus BCR-ABL1-negative MO7e leukemia cell lines. Figure 1C shows that cells expressing TKs have an approximately 2-fold increase in steady-state protein levels of c-MYC, LIG3, and PARP1 compared with controls ($P < 0.05$). In addition, c-MYC-positive control Cyclin A (CCNA2) shows an approximately 2-fold increase in TK-activated cells, whereas GRB2, which has been reported not to be controlled by c-MYC (24), is not significantly altered (Fig. 1C, bottom).

c-MYC inhibition results in decreased LIG3 and PARP1 levels in FLT3/ITD- and BCR-ABL1-positive cells

Next, to determine whether depletion of endogenous c-MYC results in decreased levels of LIG3 and PARP1 transcripts and proteins, siRNA-mediated knockdown of c-MYC was performed in MO7e-BCR-ABL1 and 32D-FLT3/ITD, followed by qPCR and Western blotting of mRNA and protein levels, respectively. To ensure that observed effects of siRNA-mediated c-MYC knockdown were not due to cell death, we performed experiments over a 48-hour period and confirmed cell viability by trypan blue dye exclusion as well as by MTS-based viability assays (Supplementary Fig. S1A and S1B). siRNA-mediated knockdown in above cell lines, using pooled oligonucleotides of c-MYC (>50%), led to a

Muvarak et al.



significant reduction ($P < 0.01$) in both mRNA and protein levels of LIG3 and PARP1 (Fig. 1D and E). Similar results were observed upon c-MYC knockdown in the FLT3/ITD-positive cell line MOLM14 (Supplementary Fig. S1C). siRNA-mediated c-MYC knockdown, using single oligonucleotides, yielded similar results to experiments using pooled oligonucleotides (Supplementary Fig. S1D). Furthermore, chemical inhibition of c-MYC [10058-F4, 60 $\mu\text{mol/L}$ (selleckchem.com)] which inhibits MYC-MAX binding and prevents transcriptional activation of c-MYC targets (25) resulted in a significant reduction of LIG3 and PARP1 transcripts (Supplementary Fig. S1E).

c-MYC induces the transcription of LIG3 and PARP1 in FLT3/ITD- and BCR-ABL1-positive cells

Database searches using MatInspector (Genomatix) and TF Search (Parallel Application TRC Laboratory) revealed several predicted c-MYC binding sites (E-box motifs) within the defined *PARP1* and *LIG3* promoter regions (Fig. 2A). In addition, ChIP-seq data from ENCODE (UCSC Genome Browser) revealed the increased binding of c-MYC to several DSB repair gene promoters, including *PARP1* and *LIG3* in the BCR-ABL1-positive cell line K562, similar to well-established c-MYC targets, *CAD* and *CCNA2* (Fig. 2B). In addition, genes reported not to be controlled by c-MYC, such as *GRB2* (24) or immediate early gene *FOS* (26), had relatively little c-MYC binding (Fig. 2B). To determine the significance of c-MYC binding to the promoters of ALT-NHEJ genes, the promoter regions of *LIG3* and *PARP1* (containing the putative c-MYC binding sites) were cloned into pGL4.10 luciferase expression plasmids. Plasmid constructs were transfected into 32D/ITD and MO7e-BCR-ABL1 cells, and induction of luciferase expression via endogenous c-MYC was determined by luciferase assay (Materials and Methods). Cells transfected with a plasmid containing either the *LIG3* or *PARP1* promoter, compared with a promoterless control vector, induced luciferase expression 4- to 25-fold (Supplementary Fig. S2A). Figure 2C shows that baseline *LIG3* and *PARP1* promoter induction of luciferase expression in MO7e-BCR-ABL1 and 32D/ITD cells was approximately 3-fold higher ($P < 0.01$) compared with that in parental control cells. Importantly, c-MYC knockdown in 32D/ITD and MO7e-BCR-ABL1 cells resulted in a significant reduction ($P < 0.05$) in promoter activity as shown in Fig. 2C.

To further confirm that c-MYC induces the transcription of the *LIG3* and *PARP1* genes, we used 2 c-MYC expression vectors described by Ricci and colleagues (21). First, pBABE-puro-mycER was transfected into MO7e-BCR-ABL1 cells which were subsequently treated with either vehicle (ethanol) or 300 nmol/L 4-hydroxytamoxifen (4-OHT). 4-OHT induces translocation of mycER from the cytoplasm to the nucleus and activation of c-MYC-mediated transcription. Induction of c-MYC resulted in

approximately a 1.7-fold ($P = 0.014$) increase in *LIG3* mRNA and a 2.5-fold ($P = 0.005$) increase in *PARP1* mRNA levels at 12 hours postinduction with 4-OHT. Cyclin D2 (*CCND2*) mRNA, which was induced approximately 2-fold ($P = 0.01$) by mycER, was used as a positive control, as Cyclin D2 was previously shown to be a downstream target of mycER-induced transcription (27). MycER protein expression was also verified by Western blot analysis (Fig. 2D). We also used a well-established c-MYC overexpression model (21) in which the c-MYC expression vector, pcDNA3-cmyc, is cotransfected into 293T cells along with *PARP1* and *LIG3* promoter luciferase constructs and luciferase activity is measured in comparison to empty vector pcDNA3 controls. c-MYC overexpression (Fig. 2E) resulted in 2.5-fold ($P = 0.013$) and 1.8-fold ($P = 0.005$) increase in *LIG3* and *PARP1* promoter activities, respectively. Notably, when compared with parental controls, *LIG3* and *PARP1* luciferase activity levels were similar to those in TK-positive cells (2- to 3-fold increase, Fig. 2C). Furthermore, site-directed mutagenesis of the highest probability c-MYC binding sites (as determined by Genomatix software) within the *LIG3* and *PARP1* promoter-reporter constructs (Fig. 2A), resulted in a significant decrease in *LIG3* (40%; $P = 0.02$) and *PARP1* (30%; $P = 0.004$) promoter activities, compared with cells transfected with wild-type promoter-reporter vectors (Fig. 2E). Importantly, cells transfected with the mutant promoter-reporter constructs showed significantly decreased luciferase activity, compared with controls (Fig. 2E). We obtained similar results as above using a promoter-reporter vector of carbamoyl-phosphate synthase 2 (*CAD*), a well-established target of c-MYC-induced transcription (28), as a positive control (Supplementary Fig. S2B).

To determine whether c-MYC actually binds to the promoters of the *LIG3* and *PARP1* genes and to confirm the ChIP-seq data (from ENCODE) observed in K562 cells (Fig. 2B), we performed ChIP in extracts from MO7e-BCR-ABL1-positive (Fig. 2F) and FLT3/ITD-positive MOLM14 cells (data not shown), followed by PCR amplification of *LIG3* and *PARP1* promoter regions spanning the putative c-MYC binding sites. qPCR analysis of ChIP products confirmed c-MYC binding to the *LIG3* and *PARP1* promoters, compared with positive (*CAD*), negative (*Ch22*), and IgG controls (Fig. 2F).

c-MYC regulation of LIG3 and PARP1 expression is dependent on expression of FLT3/ITD and BCR-ABL1

Given that c-MYC is a downstream target of the FLT3/ITD and BCR-ABL1 TKs (15, 29), we sought to investigate whether c-MYC regulation of *LIG3* and *PARP1* is dependent on the activities of these TKs. Therefore, FLT3/ITD-positive MOLM14 and MO7e-BCR-ABL1 cells were treated with TKIs (50 nmol/L of the FLT3 inhibitor CEP701 or 5 $\mu\text{mol/L}$ of the BCR-ABL1 inhibitor imatinib, respectively) or DMSO. Thereafter, qPCR analysis of mRNA

Figure 1.

c-MYC expression levels correlate with LIG3 and PARP1 levels in myeloid leukemias and are elevated in TK-positive leukemias compared to controls. Graphs of correlations between endogenous expression levels of (A) c-MYC and LIG3 or (B) c-MYC and PARP1 from microarray data of mRNAs from AML cell lines ($n = 7$) and AML primary samples ($n = 18$). Pearson (r) value denotes the strength of the correlation. C, left, top, Western blot analysis of basal protein levels for c-MYC, LIG3, and PARP1 in TK-positive cell lines and TK-negative controls (shown in pairs): REH versus MOLM14, 32D versus 32D/ITD, Mo7e versus K562, Mo7e versus MO7eBCR-ABL (MBA). Left, bottom, basal protein expression for c-MYC-positive control, cyclin A, and GRB2 reported not to be regulated by c-MYC. Actin was used as a loading control. Right, graphical representation of protein expression relative to control in 3 independent Western blot analyses. Error bars represent SD. Statistical significance was determined using the Student t test. D and E, siRNA-mediated knockdown of c-MYC (siMYC) and controls (siCTRL) in TK-activated cell lines and examination LIG3 and PARP1 expression levels by PCR in (left) 32D-FLT3/ITD and (right) MO7e-BCR-ABL1 cell lines. Columns represent the average fold decrease in mRNA expression relative to each control, and error bars denote SD (E). Left, representative Western blot analysis of c-MYC, LIG3, and PARP1 proteins. Right, graphical representation of 3 independent experiments. Columns represent the average of 3 different experiments. Error bars represent SD. Statistical significance was determined using the Student t test.

Muvarak et al.

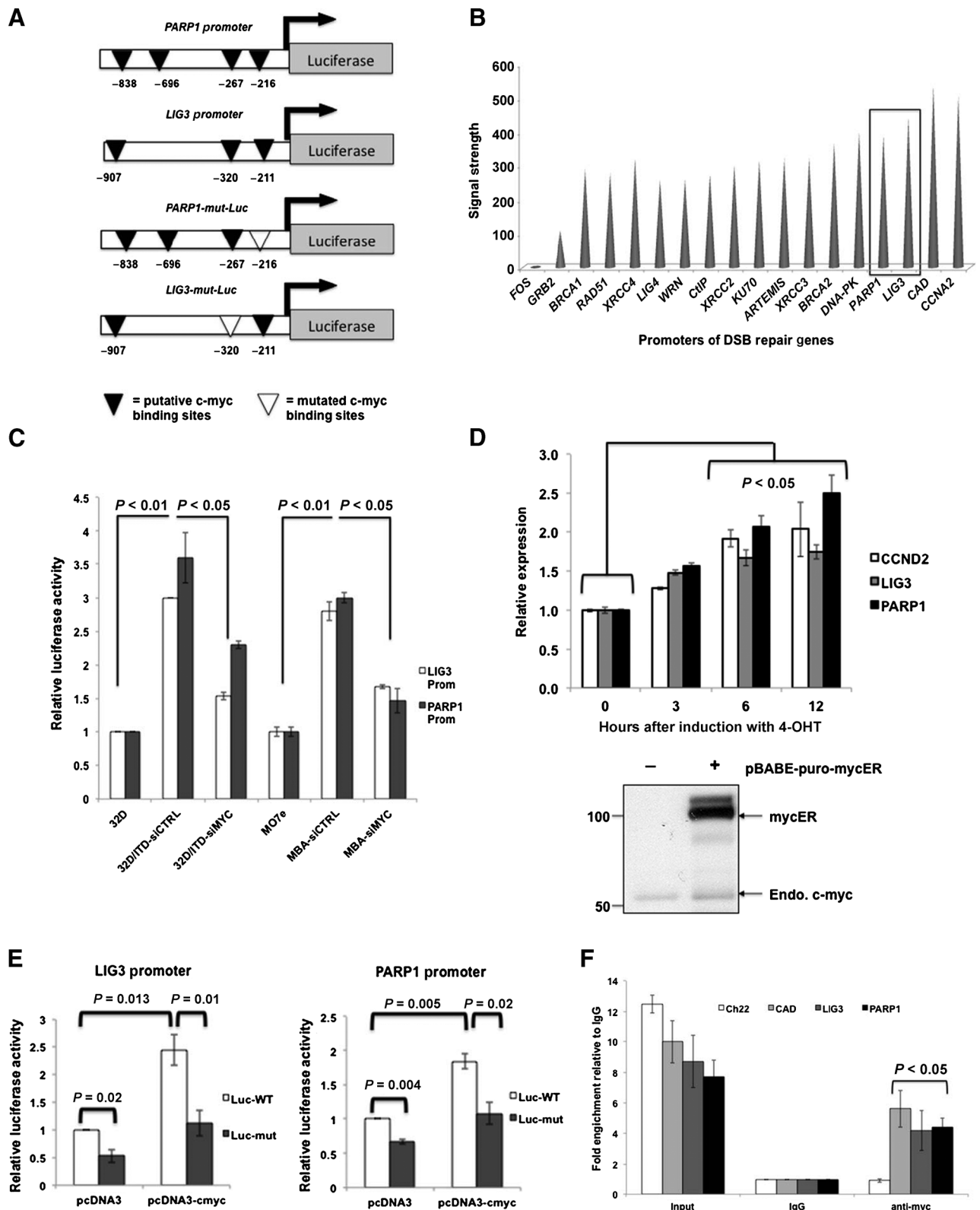


Figure 2.

c-MYC induces the transcription of LIG3 and PARP1 in FLT3/ITD- and BCR-ABL1-positive cells. A, schematic diagram of PARP1 and LIG3 promoters cloned into pGL4.10 luciferase construct. Black inverted triangles represent the putative c-MYC binding sites within each cloned promoter, and empty triangles represent c-MYC binding sites that were mutated by site-directed mutagenesis. (Continued on the following page.)

and Western blot analysis of protein levels were performed. FLT3/ITD inhibition resulted in greater than 75% ($P < 0.005$) decrease in c-MYC, LIG3, and PARP1 mRNA levels (Fig. 3A and B). Imatinib treatment of MO7e-BCR-ABL1 cells resulted in smaller (20%–30%) yet significant decrease ($P < 0.04$) in mRNA and protein levels of c-MYC, LIG3, and PARP1 (Fig. 3A and B). As seen in Fig. 3C, TKI treatment of MOLM14 and MO7e-BCR-ABL1 resulted in similar effects on the protein levels of LIG3 and PARP1 as was observed for mRNA levels (Fig. 3A and B). Of note, we did not observe the presence of cleaved PARP1 (Fig. 3C), suggesting that the downregulation observed was not a result of the cells undergoing apoptosis. To ensure that PARP1 can undergo cleavage at this time point, we treated cells with 50 nmol/L (MOLM14) or 1 μ mol/L (MO7e-BCR-ABL1) etoposide and demonstrated PARP1 cleavage (Fig. 3D). Given that c-MYC phosphorylation at Serine 62 (Ser62) is an indication of its signaling activity (30), we performed Western blotting for this c-MYC phosphorylation site following treatment with the TKIs described above and showed that phospho-Ser62 is decreased significantly following treatment in both cell lines (Fig. 3E).

c-MYC negatively regulated miRNAs decrease LIG3 and PARP1 expression in FLT3/ITD- and BCR-ABL1-positive cells

c-MYC is known to specifically regulate expression of multiple miRNAs, the majority of which undergo negative regulation by this transcription factor (19). To determine whether c-MYC-mediated decrease in miRNA levels in leukemia cells may be an additional mechanism of LIG3 and PARP1 regulation, we examined the 3'-untranslated region (UTR) and coding sequences of LIG3 and PARP1 for potential c-MYC-regulated miRNA binding sites (Supplementary Table S2). LIG3 and PARP1 are predicted targets of multiple c-MYC-regulated miRNAs, including miR-22, miR-27a, miR-34a, and miR-150. In our initial studies, we used microarray analysis of mRNA expression and mature miRNA levels from multiple AML cell lines and primary samples (Supplementary Table S1) shown in Fig. 1A and B, to look for a correlative relationship between LIG3 or PARP1 and the above miRNAs. There was a significant inverse correlation between LIG3 and miR-22 and -150 (Pearson $r < -0.3$, Fig. 4A); similarly, there is a significant inverse correlation between PARP1 and miR-22 and -150 (Pearson $r < -0.3$, Fig. 4B). Not surprisingly, there was a significant inverse correlation between c-MYC and miR-22 and -150 (Pearson $r < -0.3$, Fig. 4C). In contrast, miR-34a showed neither a positive nor inverse correlation with either LIG3 or PARP1 (Supplementary Fig. S3A). While miR-27a demonstrated an inverse correlation with PARP1, it did not significantly correlate with LIG3 (Supplementary Fig. S3B). Accordingly, we focused on miR-22 and -150 for the remainder of this study.

First, we sought to confirm c-MYC repression of miR-22 and -150 in our cell lines. We performed siRNA-mediated knockdown of c-MYC in 3 different cell lines (MOLM14, K562, and MO7e-BCR-ABL1) followed by qRT-PCR analysis of miR-22 and -150 levels. There was a significant increase in levels of miR-22 and/or -150 in cells transfected with siRNA targeting c-MYC, compared with cells transfected with control siRNA (Supplementary Fig. S3C). To confirm that miR-22 and -150 are involved in regulating the expression of LIG3 and PARP1 in TK-activated leukemias, we transiently transfected a combination of miR-22 and miR-150 mimics (50 nmol/L each) into MOLM14 and MO7e-BCR/ABL cells and assessed LIG3 and PARP1 protein levels at 72 hours posttransfection. We verified the transfection efficiency and confirmed high levels of miRs by qPCR in several cell lines (Supplementary Fig. S3D). Transfection of a combination of miR-22 and -150 produced an approximately 35% to 40% decrease in LIG3 ($P < 0.05$) and PARP1 ($P < 0.05$) protein levels, respectively, compared with MOLM14, and MO7e-BCR-ABL1 cells transfected with a non-specific control (NSC) miRNA (Fig. 4D and E).

Depletion of c-MYC and overexpression of c-MYC-regulated miR-150 and miR-22 decrease ALT-NHEJ activity in FLT3/ITD- and BCR-ABL1-positive cells

To determine whether c-MYC regulation of key ALT-NHEJ components in TK-activated leukemias also plays a role in ALT-NHEJ repair activity, we performed an established *in vivo* plasmid-based end-joining assay (11, 12, 31, 32) following chemical and siRNA inhibition of c-MYC. In this assay (Fig. 5A), pUC18 plasmid is linearized by restriction enzyme digestion to simulate a DSB and then transfected into cells. The repaired plasmids are isolated from cells and transformed into DH5 α bacteria, which are then plated on agar plates. Colonies (representing clones of one repaired plasmid) are picked for plasmid isolation and sequencing of repair junctions. c-MYC was inhibited in MOLM14 and MO7e-BCR/ABL1 using chemical inhibition (10058-F4) or siRNA technology, followed by the above end-joining assays. c-MYC knockdown and consequent decrease in LIG3 and PARP1 levels were confirmed by Western blot analysis (Supplementary Fig. S4A and S4B). We also verified that the transfection efficiency of the linearized pUC18 plasmid was not affected by c-MYC knockdown by cotransfection with a GFP-expressing vector (Supplementary Fig. S4C). Approximately 30 colonies from 3 independent experiments were analyzed by colony PCR and sequencing of the region that encompasses the repaired DSB. MOLM14 cells depleted of c-MYC by chemical inhibition had a general reduction in the size of DNA deletions when compared with DMSO-treated cells (Fig. 5B, $P < 0.015$).

(Continued.) B, ChIP-Seq data in K562 cells obtained from ENCODE show c-MYC binding to the promoters of several DSB repair genes, c-MYC targets, and genes not regulated by c-MYC. Peak heights represent the signal strength, with LIG3 and PARP1 (rectangle) exhibiting high levels of c-MYC binding similar to positive controls, CAD and CCNA2. Negative controls Fos and GRB2 are also shown. C, luciferase assays conducted in 32D, 32D/ITD, MO7e, and MO7e-BCR/ABL (MBA) cells transfected with either siRNAs against MYC (siMYC) or controls siRNA (siCtrl) and cotransfected with the LIG3 or PARP1 promoter constructs. Values shown are relative luciferase activity (FF) normalized to Renilla (RL) that served as a control for transfection efficiency. Columns represent the average of 3 independent assays and the error bar represents SD. D, c-MYC induction by qPCR analysis of mRNA from MO7e-BCR-ABL1 cells transfected with pBabe-puro-mycER and treated with either 300 nmol/L 4-OHT or ethanol (vehicle control) for the indicated times (x-axis). mRNA expression levels of LIG3, PARP1, and positive control CCDN2 (y-axis) are shown for 4-OHT-treated cells relative to vehicle controls. The inset below the graph is a representative Western blot analysis showing expression of mycER (~97 kDa). Molecular weight (kDa) markers are shown. E, luciferase activity of transfected LIG3 and PARP1 wild-type (luc-WT) and mutant (luc-mut) promoter constructs in 293T cells co-transfected with either control pcDNA3 or pcDNA3-cmyc. The error bar represents SD. Statistical significance was determined using the Student *t* test. F, ChIP of LIG3 and PARP1 in MO7e-BCR-ABL1 cells. qPCR analysis of mRNA from cells immunoprecipitated with myc antibody (N-262), positive control CAD, or negative control chromosome 22 region (Ch22) or IgG antibody. Graphical representation of fold enrichment relative to IgG controls from 3 independent ChIP assays. The error bar represents SD. Statistical significance ($P < 0.05$) was determined using the Student *t* test.

Muvarak et al.

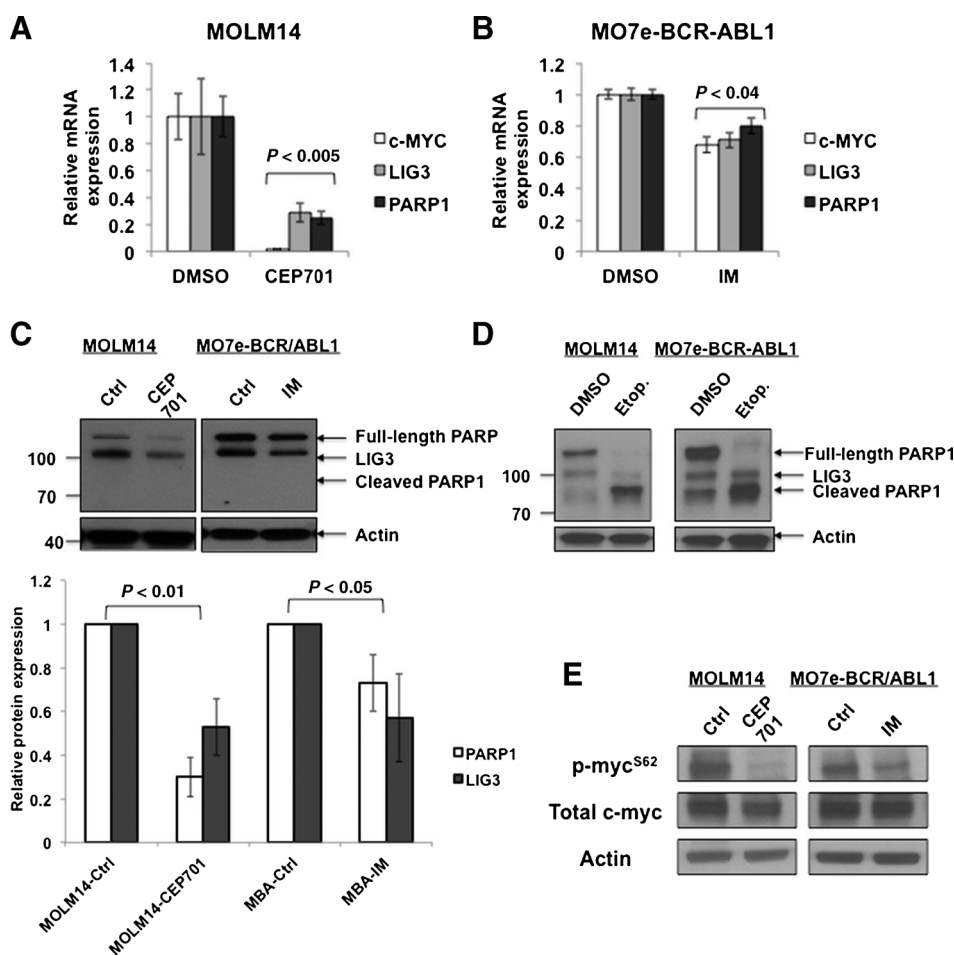


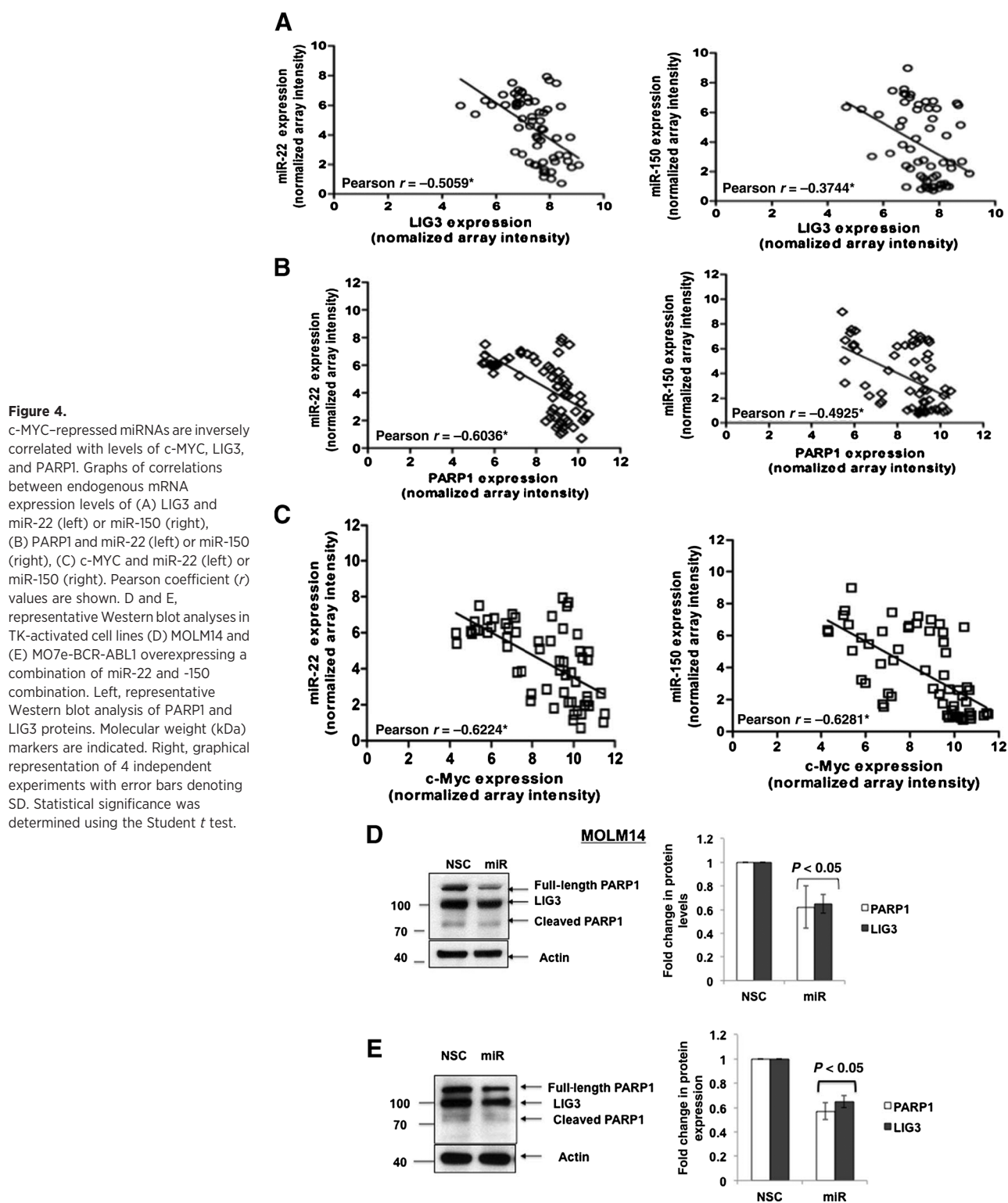
Figure 3. Treatment with TKIs reduces levels of PARP1 and LIG3 in AML and CML cell lines. Expression levels of c-MYC, LIG3, and PARP1 in TK-activated cell lines treated with 50 nmol/L CEP701 and 5 μ mol/L imatinib (IM) or DMSO (controls) followed by mRNA extraction and qPCR analysis. Relative expression of mRNA in (A) MOLM14 cells and (B) MO7e-BCR-ABL1. The error bar represents SD. Statistical significance was determined using the Student *t* test. C, top, representative Western blot analysis of LIG3 and PARP1 proteins. Bottom, graph representation of relative protein expression levels from 3 independent experiments. D, Western blot analysis for PARP cleavage following treatment with etoposide. E, Western blot analysis for c-MYC phosphorylation at serine 62 (p-myc^{S62}) and total c-MYC. Actin was used as a loading control in C-E.

Similar results were obtained following siRNA-mediated knockdown of c-MYC in MO7e-BCR-ABL1 cells (Fig. 5C, $P < 0.05$). Importantly, repair assays performed with linearized pUC18 DNA controls showed very few colonies (Supplementary Fig. S4D). In addition, we analyzed the data for the proportion of large deletions (>20 bp) versus small deletions (<20 bp) that are characteristic of c-NHEJ (Supplementary Fig. S4E). Approximately 50% of DSBs are repaired in TK-activated cell lines MOLM14 and MO7e-BCR-ABL1 with small deletions occurring at the repair junctions. Following siRNA knockdown of c-MYC, the fraction of small deletions actually increases significantly (Supplementary Fig. S4E). In fact, siRNA knockdown of c-MYC results in a slight but insignificant increase in NHEJ efficiency using a different NHEJ reporter (pEGFP-Pem1-Ad2) assay (Fattah, 2010, #11559). In contrast, knockdown of control c-NHEJ factor, LIG4, reduces NHEJ efficiency significantly (Supplementary Fig. S4F and S4G). This suggests that c-MYC may not contribute significantly to c-NHEJ activity. Moreover, c-MYC depletion decreased the frequency of microhomology-mediated repair (Fig. 5D, $P < 0.05$). Notably, overexpression of miR-150 and miR-22 in MO7e-BCR-ABL1 cells produced the same results seen with c-MYC inhibition (Fig. 5E and F). The reduction in LIG3 and PARP1 protein levels after miR overexpression was confirmed by Western blot analysis (Supplementary Fig. S4H).

c-MYC mRNA levels correlate with LIG3 and PARP1 mRNA and inversely correlate with miR-22 and -150 in primary samples from patients with CML

To determine whether primary CML samples demonstrated increased expression levels of c-MYC and decreased levels of miR-150 and -22, we first examined mRNA samples from 21 patients with CML (Table 1) and compared transcript levels of c-MYC, LIG3, and PARP1 in peripheral blood and bone marrow bone marrow mononuclear cells (BMMNC) samples with those of normal bone marrow (NBM) controls. As seen in Fig. 6A and B, there was a strong positive correlation between c-MYC mRNA levels and LIG3 (Pearson $r = 0.88$, $P < 0.001$) and PARP1 (Pearson $r = 0.84$, $P < 0.001$) mRNA levels. c-MYC expression was increased in 12 of 21 samples (57%), compared with normal controls. Of the 12 CML samples with increased c-MYC levels, 9 (75%) also had increased levels of LIG3 and PARP1 (Table 1). In these samples with increased levels of c-MYC, PARP1, and LIG3, there was no bias toward a particular disease phase or response to TKIs. Interestingly, however, 2 of 3 TKI-resistant patients with CML (Table 1, PT #8 and #16) with T315I-BCR-ABL1 mutations (34, 35) had increased levels of c-MYC, LIG3, and PARP1.

CML patient samples were next evaluated for expression of c-MYC-regulated miRs. We first examined mRNA for miR-150 in a subset of the above-described patient samples ($n = 8$; Table 1, PT #6, #8, #13, #17, #18, #20, #21) for which mRNA was available



and 2 additionally acquired patients with CML (Supplementary Table S3; #22 in chronic phase and #23 in blast crisis) by miRNA qPCR analysis and compared results with NBM ($n = 2$). There was a significant decrease ($P < 0.05$) in c-MYC-repressed miR-150 levels in all CML samples, compared with NBM (Fig. 6C). We

next examined miR-22 expression levels in CML patient samples in chronic phase ($n = 4$; Supplementary Table S3; PT #13, #24, #25, and #26) versus those in blast crisis ($n = 4$; Supplementary Table S3; #8, #18, #20, and #23). In contrast to results with miR-150, miR-22 expression levels appear to be decreased significantly

Muvarak et al.

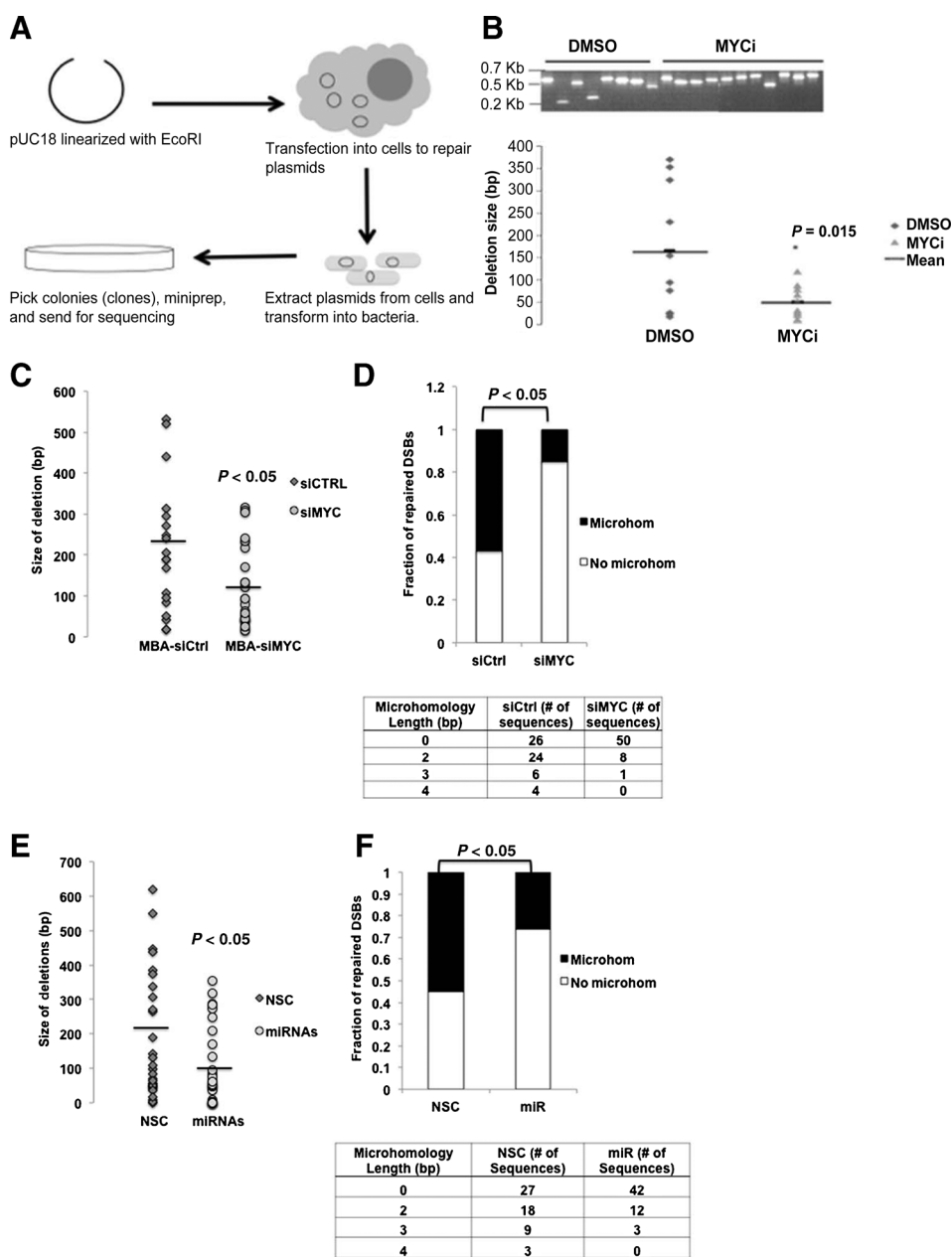


Figure 5. c-MYC inhibition and miR-22/150 overexpression results in decreased ALT-NHEJ activity in TK-positive cell lines. A, schematic diagram of the NHEJ assay. A DSB is created with a restriction-enzyme (*EcoRI*) digest of pUC18 plasmid. The linearized plasmid is transfected into treated cells to allow repair. After 24 hours, the repaired plasmids are harvested and transformed in *E. coli* and plated on LB agar plates. Clones are isolated for plasmid DNA extraction and sequencing of repair junctions. B, NHEJ assay in MOLM14 cells treated with either DMSO or 30 $\mu\text{mol/L}$ c-MYC inhibitor 10058-F4 (MYCi). Top, representative agarose gel of PCR products of plasmid DNA isolated from DMSO- or 10058-F4 (MYCi)-treated cells. Bottom, graphical representation of the size of deletions determined by sequencing of the repair junctions in individual plasmid DNAs represented by symbols. The average size of deletion (in bp) is indicated by a horizontal black line. C-F, end-joining experiments in MO7e-BCR-ABL1 cells depleted of c-MYC by siRNA technology or using siRNA controls (C and D) or overexpressing a combination of miR-22 and miR-150 (E and F). C and E, graphical representation of deletion sizes determined by sequencing of the repair junctions. Individual sequenced plasmid DNAs are represented by symbols. The average size of deletion (in bp) is indicated by a horizontal black line. D and F, plasmids sequences analyzed for DNA sequence microhomology and graphed as fractions of DNA sequences that exhibited microhomologies (>2 bp) (Microhom) or no microhomology-mediated repair (No Microhom). The table below the graph summarizes plasmid sequences analyzed from experiment and control groups, according to the lengths of microhomologies.

($P < 0.01$) in patients with CML-BC when compared with patients with CML-CP (Fig. 6D). To confirm these data, we analyzed NanoString miR expression arrays from a separate cohort of CML patient mRNAs from paired MNC samples of patients with CML-CP ($n = 5$) and -BC ($n = 5$) healthy donor (HD) controls ($n = 3$). As expected from the earlier correlation studies (Supplementary Fig. S3B), miR-27a showed no significant differences in expression between CML patient samples and healthy donor controls (Fig. 6E). In contrast, and as seen in the first cohort of CML patient samples (Fig. 6C), levels of miR-150 were significantly decreased in both chronic phase and blast crisis compared with healthy donors, and there were no significant expression differences between chronic phase and blast crisis in the 5 paired patient samples examined (Fig. 6E). Similar to the above results (Fig. 6D),

compared with healthy donor controls, miR-22 expression was decreased significantly only in blast crisis, compared with healthy donor controls (Fig. 6E).

Discussion

Leukemia cells expressing constitutively activated BCR-ABL1 or FLT3/ITD TKs are characterized by a highly error-prone and alternative form of NHEJ (ALT-NHEJ) involving increased expression of LIG3 and PARP1, that is likely responsible for much of the error-prone end-joining repair (12, 14). To date, the mechanism through which TKs activate ALT-NHEJ factors had not been elucidated. Our studies have, for the first time, linked c-MYC, a key downstream target of both BCR-ABL1 and FLT3/ITD to

Table 1. Clinical and molecular features of patients with CML

Patient	Phase	Mutations	IM status	LIG3 up	PARP1 up	c-MYC up
1	Chronic	None	Sensitive	Y	Y	Y
2	Chronic	None	Sensitive	Y	Y	N
3	Chronic	None	Resistant	Y	Y	Y
4	Chronic	None	Sensitive	Y	N	N
5	Chronic	None	Sensitive	N	N	N
6 ^a	Blast crisis	None	Resistant	Y	Y	Y
7	Blast crisis	None	Resistant	N	N	N
8 ^a	Blast crisis	T315I	Resistant	Y	Y	Y
9	Accelerated	None	Resistant	N	N	N
10	Unknown	Unknown	Unknown	N	Y	Y
11	Chronic	None	Resistant	Y	Y	Y
12	Chronic	None	Resistant	Y	Y	Y
13 ^a	Chronic	None	Sensitive	Y	Y	Y
14	Chronic	None	Sensitive	Y	Y	Y
15	Blast crisis	None	Resistant	N	Y	N
16	Blast crisis	T315I	Resistant	Y	Y	Y
17 ^a	Blast crisis	None	Sensitive	N	N	N
18 ^a	Blast crisis	None	Resistant	N	N	N
19 ^a	Chronic	None	Sensitive	N	N	Y
20 ^a	Blast crisis	None	Resistant	N	N	N
21 ^a	Blast crisis	T315I	Resistant	N	N	Y

NOTE: Increased LIG3, PARP1 and c-MYC expression relative to normal control bone marrow MNC and based on $P < 0.05$ by the t test.

Abbreviations: IM, imatinib; N, no; Y, yes.

^aPatient samples used for miRNA analysis.

increased expression of the ALT-NHEJ factors LIG3 and PARP1 and increased ALT-NHEJ repair activity.

While elevated expression of c-MYC occurs frequently in human cancers and is associated with tumor progression and poor clinical outcome (36), the effect of high levels of c-MYC on global gene regulation is poorly understood. Recent studies suggest that high levels of c-MYC accumulate in the promoter regions of active genes and cause transcriptional amplification, producing increased levels of transcripts within the cell's gene expression program (37). Our studies demonstrate that c-MYC binds to the promoter regions of both LIG3 and PARP1, thereby increasing transcriptional activity, leading to increased ALT-NHEJ in TK-activated cells. Thus, ALT-NHEJ activity, which is present at low levels in normal cells (11), is increased through transcriptional activity of the key pathway components LIG3 and PARP1, likely leading to acquisition of genomic alterations. Given the role of c-MYC in cell-cycle progression, the possibility exists that the expression of PARP1 and LIG3 and therefore ALT-NHEJ may be influenced by the cell cycle. Studies performed in cells enriched for particular phases of the cell cycle should clarify this question. Given that c-MYC is known to bind several DSB repair genes (18), increased expression of LIG3 and PARP1 may be part of a dysregulated expression program involving abnormal DSB repair that leads to genomic instability. Therefore, similar studies are merited for other DSB repair genes. Thus, while increased ALT-NHEJ activity may be a plausible mechanism for genomic instability, and studies that measure actual chromosomal instability are warranted (38).

The most extensively used point of gene regulation is at the level of transcription, whereas miRNAs are thought to be involved in "fine-tuning" gene regulation. miRNAs are involved in the regulation of many cancer-specific signaling pathways in hematopoiesis and are aberrantly expressed in hematologic malignancies (39). c-MYC is known to negatively regulate a group of miRNAs, which is thought to contribute to tumorigenesis (19). In the context of LIG3 and PARP1 regulation, we propose in addition to its transcriptional regulation of these genes, c-MYC also

represses miRNAs (miR-22 and miR-150) that target LIG3 and PARP1 transcripts. Indeed, this dual regulation by c-MYC was previously reported; c-MYC was shown to regulate the transcription factor E2F1 through direct transcription and activation of miRNAs that target E2F1 (40). Another group showed that expression of EZH2, a protein involved in regulation of gene expression, was amplified as a result of c-MYC-mediated repression of miR-26a, which targets EZH2 (41).

We previously reported that treatment of BCR-ABL1- and FLT3/ITD-positive cells with TK inhibitors leads to decreased expression of the ALT-NHEJ components LIG3 and PARP1 (8, 13, 14) and decreased DSB repair errors, indicating that the altered DNA repair is due to one or more of the effectors of these signaling pathways (12). Our studies here show that the downstream TK target c-MYC mediates expression of the ALT-NHEJ factors PARP1 and LIG3 that is dependent on BCR-ABL1 or FLT3/ITD. Furthermore, our studies demonstrate that the TKI CEP-701 strongly downregulates expression of c-MYC, LIG3, and PARP1 in FLT3/ITD-positive cells, compared with a weaker effect of imatinib in BCR-ABL1-positive cells. One explanation is that the mechanisms of drug action of the specific inhibitors may differ. Whereas imatinib targets BCR-ABL1 activity, studies have shown that CEP701 inhibits FLT3 and Jak2 (42), both of which are important for c-MYC activity (15, 29). Another explanation may be that the mechanisms of c-MYC activation may differ in the 2 models of TK-activated leukemia. In Bcr-Abl1-positive leukemias, Jak2 mediates the increase c-MYC RNA expression but also interferes with proteasome-dependent degradation of c-Myc protein (29, 43). In contrast to studies in BCR-ABL1-positive cells, while gene expression induced by FLT3/ITD or constitutively activated wild-type FLT3 signaling induces high expression levels of c-MYC (15), few mechanistic studies have been reported to elucidate how c-MYC is regulated by FLT3/ITD.

Previous studies demonstrate that c-MYC expression increases as CML progresses to blast crisis, and this overexpression induces aberrant DNA synthesis, suggesting a role for c-MYC in disease progression through promoting genomic instability (44). Our

Muvarak et al.

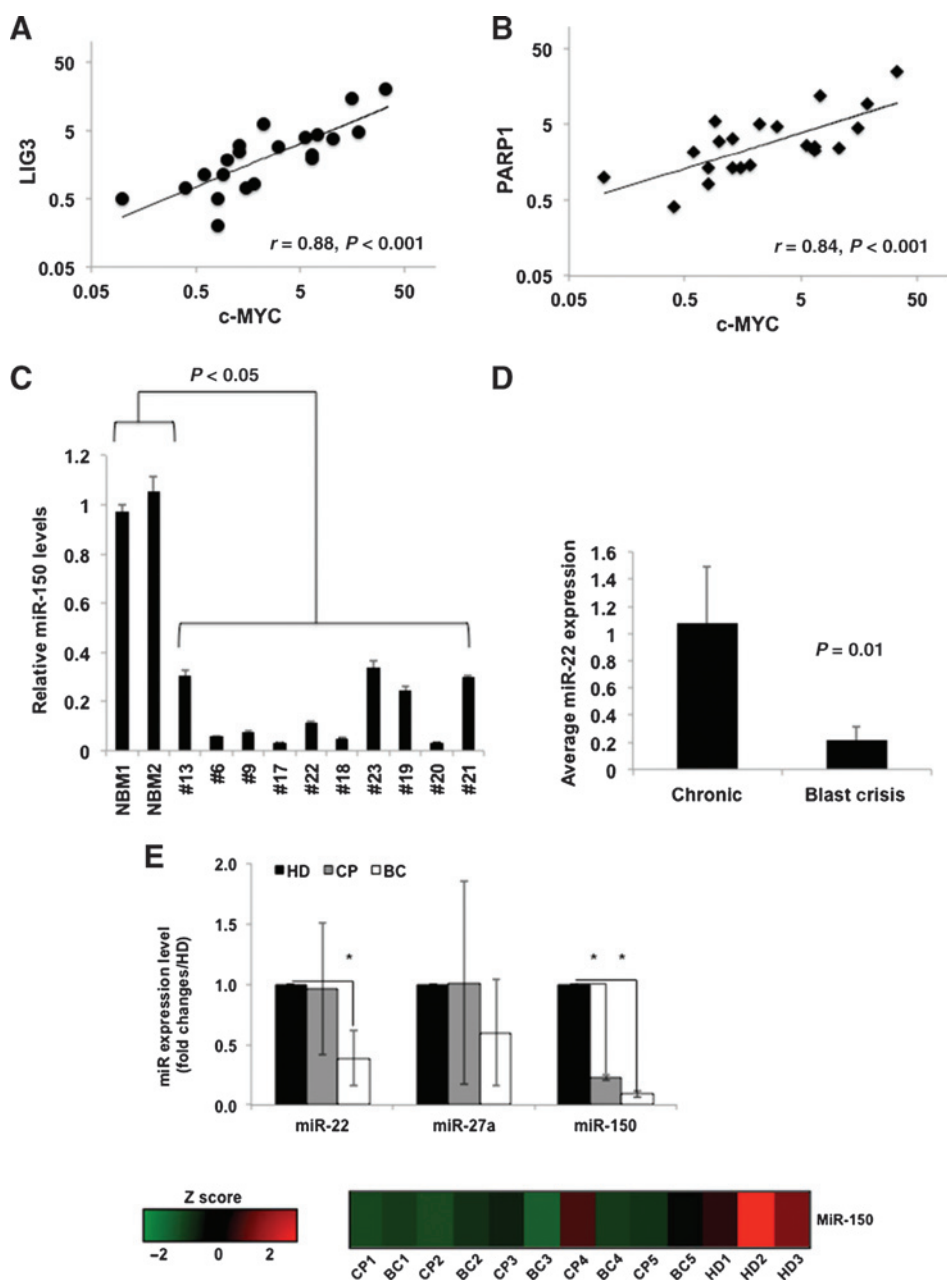


Figure 6. c-MYC levels strongly correlate with LIG3 and PARP1 levels, and miR-22 and miR-150 are reduced in primary CML patient samples. Graphical representation of correlations between mRNA expression levels of (A) c-MYC (x-axis) and LIG3 (y-axis) and (B) c-MYC (x-axis) and PARP1 (y-axis) in 21 CML patient samples (Table 1). Pearson correlation values (r) are shown. C, relative expression levels of miR-150 from CML patient samples ($n = 10$) and normal bone marrow (NBM1 and NBM2) from healthy individuals. Error bars represent SD from 3 independent PCR analyses. Statistical significance was determined using the Student t test. D, average expression levels of miR-22 in CML patient samples by phase of disease: CP and BC. E, expression levels of miR-22, -27a, and -150 in MNC from 5 matched CML patient samples in CP and BC, compared with 3 HD using Nanostring Technologies and nCounter Analysis. Top, relative mRNA expression represented as fold changes compared with HD. CP (gray bars), BC (white bars), expression levels HD (black bars) \pm SD (error bars). *, $P < 0.005$ based on the Student t test. Bottom, heatmap for miR-150 in 5 CP, 5 BC, and 3 HD samples. z-score was used to determine relative colors (green, low expression; black, no difference; red, high expression) for each sample in the heatmap.

studies shows that in the majority (75%) of CML patient samples (irrespective of disease stage) with increased c-MYC expression, LIG3 and PARP1 expression is also increased. This suggests that increased ALT-NHEJ is promoted throughout the course of CML disease. However, in a minority (25%) of primary CML samples, c-MYC expression is not correlated with LIG3 and PARP1 expression, suggesting that additional molecular mechanisms may be involved in regulating LIG3 and PARP1 and ALT-NHEJ. Expression of miR-150 which is negatively regulated by c-MYC was significantly decreased (compared with normal bone marrow) in all CML patient samples tested, regardless of disease stage, suggesting that miR-150 is repressed in a BCR-ABL1-dependent manner (45). In contrast, miR-22 appears to be preferentially decreased in patients with CML-BC. One study

(46) demonstrated a role for miR-22 in inducing cellular senescence, thereby preventing cancer progression. Considering that one of the hallmarks of blast crisis is increased genomic instability, it is tempting to speculate that miR-22 suppression in blast crisis may override DNA damage-induced senescence, leading to promotion of genomic instability. Studies into the exact function of miR-22 in blast crisis with respect to genomic instability would be of particular interest.

Published studies also demonstrate higher c-MYC expression in samples from patients not responding to imatinib therapy, compared with those responding to therapy (44). Interestingly, 2 of 3 bone marrow samples with T315I mutations, connoting the greatest resistance to TKIs showed elevated steady-state levels of c-MYC, LIG3, and PARP1. Therefore, increased ALT-NHEJ may

exist in a cellular milieu of increased c-MYC activity in which multiple aberrant repair pathways are active, leading to acquisition of TKI-resistant BCR-ABL1 mutations.

From a therapeutic standpoint, targeting c-MYC in leukemia may not be a viable option, considering the myriad of roles c-MYC plays in normal cells. However, the identification of other "druggable" downstream targets of c-MYC may be considered. With respect to our current study, PARP1 represents an attractive target for therapy, as PARP1 inhibitors are currently used in the clinic, and new ones are being investigated in clinical trials. In fact, a recent study by our collaborators demonstrated that PARP1 inhibition is synthetically lethal in TK-driven leukemias that exhibit defects in the HR pathway (47). Therefore, given that DSBs are lethal if not repaired, the c-MYC downstream targets LIG3 and PARP1 and other DSB repair factors may be attractive targets for therapy (48).

Disclosure of Potential Conflicts of Interest

No potential conflicts of interest were disclosed.

Authors' Contributions

Conception and design: N. Muvarak, C. Gambacorti-Passerini, C. Civin, F. Rassool

Development of methodology: K. Scheibner

Acquisition of data (provided animals, acquired and managed patients, provided facilities, etc.): S. Kelley, M.R. Baer, D. Perrotti

Analysis and interpretation of data (e.g., statistical analysis, biostatistics, computational analysis): N. Muvarak, S. Kelley, C. Robert, K. Scheibner, F. Rassool

Writing, review, and/or revision of the manuscript: N. Muvarak, M.R. Baer, C. Civin, F. Rassool

Administrative, technical, or material support (i.e., reporting or organizing data, constructing databases): S. Kelley

Study supervision: N. Muvarak, C. Gambacorti-Passerini, F. Rassool

Acknowledgments

The authors thank Jason G. Harb, Paolo Neviani, and Justin Ellis (Ohio State University, Columbus, OH) for scientific and technical assistance with the NanoString array preparation and data analysis.

Grant Support

This work was supported by Cigarette restitution funds of Maryland (F. Rassool), NIH grants CA095512 and CA163800 (D. Perrotti), The CARIPLo Foundation Biomedical Scientific Research (C. Gambacorti-Passerini and D. Perrotti), MSCRF (K. Scheibner and S. Kelley), and by NCI Cancer Center Grant P30 CA134274.

The costs of publication of this article were defrayed in part by the payment of page charges. This article must therefore be hereby marked *advertisement* in accordance with 18 U.S.C. Section 1734 solely to indicate this fact.

Received July 28, 2014; revised November 17, 2014; accepted December 7, 2014; published OnlineFirst March 30, 2015.

References

- Sallmyr A, Fan J, Rassool FV. Genomic instability in myeloid malignancies: increased reactive oxygen species (ROS), DNA double strand breaks (DSBs) and error-prone repair. *Cancer Lett* 2008;270:1–9.
- Muvarak N, Nagaria P, Rassool FV. Genomic instability in chronic myeloid leukemia: targets for therapy? *Curr Hematol Malig Rep* 2012;7:94–102.
- Hartlerode AJ, Scully R. Mechanisms of double-strand break repair in somatic mammalian cells. *Biochem J* 2009;423:157–68.
- Khanna KK, Jackson SP. DNA double-strand breaks: signaling, repair and the cancer connection. *Nat Genet* 2001;27:247–54.
- Lieber MR. The mechanism of human nonhomologous DNA end joining. *J Biol Chem* 2008;283:1–5.
- Nussenzweig A, Nussenzweig MC. A backup DNA repair pathway moves to the forefront. *Cell* 2007;131:223–5.
- Iliakis G. Backup pathways of NHEJ in cells of higher eukaryotes: cell cycle dependence. *Radiother Oncol* 2009;92:310–5.
- Li L, Zhang L, Fan J, Greenberg K, Desiderio S, Rassool FV, et al. Defective nonhomologous end joining blocks B-cell development in FLT3/ITD mice. *Blood* 2011;117:3131–9.
- Slupianek A, Schmutte C, Tomblin G, Nieborowska-Skorska M, Hoser G, Nowicki MO, et al. BCR/ABL regulates mammalian RecA homologs, resulting in drug resistance. *Mol Cell* 2001;8:795–806.
- Seedhouse CH, Hunter HM, Lloyd-Lewis B, Massip AM, Pallis M, Carter GI, et al. DNA repair contributes to the drug-resistant phenotype of primary acute myeloid leukaemia cells with FLT3 internal tandem duplications and is reversed by the FLT3 inhibitor PKC412. *Leukemia* 2006;20:2130–6.
- Sallmyr A, Tomkinson AE, Rassool FV. Up-regulation of WRN and DNA ligase IIIalpha in chronic myeloid leukemia: consequences for the repair of DNA double-strand breaks. *Blood* 2008;112:1413–23.
- Tobin LA, Robert C, Rapoport AP, Gojo I, Baer MR, Tomkinson AE, et al. Targeting abnormal DNA double-strand break repair in tyrosine kinase inhibitor-resistant chronic myeloid leukemias. *Oncogene* 2013;32:1784–93.
- Li L, Robert C, Rassool FV. The role of error-prone alternative non-homologous end-joining in genomic instability in cancer. In: *DNA repair and human health*. 2011;Book: "DNA Repair and Human Health". Publisher: InTech. Location: Croatia, ISBN: 978-953-307-612-6.
- Fan J, Li L, Small D, Rassool F. Cells expressing FLT3/ITD mutations exhibit elevated repair errors generated through alternative NHEJ pathways: implications for genomic instability and therapy. *Blood* 2010;116:5298–305.
- Kim KT, Baird K, Davis S, Piloto O, Levis M, Li L, et al. Constitutive Fms-like tyrosine kinase 3 activation results in specific changes in gene expression in myeloid leukaemic cells. *Br J Haematol* 2007;138:603–15.
- Sawyers CL. Molecular consequences of the BCR-ABL translocation in chronic myelogenous leukemia. *Leuk Lymphoma* 1993;11 Suppl 2:101–3.
- Delgado MD, Leon J. Myc roles in hematopoiesis and leukemia. *Genes Cancer* 2010;1:605–16.
- Luoto KR, Meng AX, Wasylshen AR, Zhao H, Coackley CL, Penn LZ, et al. Tumor cell kill by c-MYC depletion: role of MYC-regulated genes that control DNA double-strand break repair. *Cancer Res* 2010;70:8748–59.
- Chang TC, Yu D, Lee YS, Wentzel EA, Arking DE, West KM, et al. Widespread microRNA repression by Myc contributes to tumorigenesis. *Nat Genet* 2008;40:43–50.
- Lozzio CB, Lozzio BB, Feliu AS, Bamberger EG. Human myeloid cell lines. *Blood* 1981;57:979–80.
- Ricci MS, Jin Z, Dews M, Yu D, Thomas-Tikhonenko A, Dicker DT, et al. Direct repression of FLIP expression by c-myc is a major determinant of TRAIL sensitivity. *Mol Cell Biol* 2004;24:8541–55.
- Geiss GK, Bumgarner RE, Birditt B, Dahl T, Dowidar N, Dunaway DL, et al. Direct multiplexed measurement of gene expression with color-coded probe pairs. *Nat Biotechnol* 2008;26:317–25.
- Scheibner KA, Teaboldt B, Hauer MC, Chen X, Cherukuri S, Guo Y, et al. MiR-27a functions as a tumor suppressor in acute leukemia by regulating 14-3-3theta. *PLoS One* 2012;7:e50895.
- Notari M, Neviani P, Santhanam R, Blaser BW, Chang JS, Galiotta A, et al. A MAPK/HNRPK pathway controls BCR/ABL oncogenic potential by regulating MYC mRNA translation. *Blood* 2006;107:2507–16.
- Loven J, Orlando DA, Sigova AA, Lin CY, Rahl PB, Burge CB, et al. Revisiting global gene expression analysis. *Cell* 2012;151:476–82.
- Nie Z, Hu G, Wei G, Cui K, Yamane A, Resch W, et al. c-Myc is a universal amplifier of expressed genes in lymphocytes and embryonic stem cells. *Cell* 2012;151:68–79.

Muvarak et al.

27. Vafa O, Wade M, Kern S, Beeche M, Pandita TK, Hampton GM, et al. c-Myc can induce DNA damage, increase reactive oxygen species, and mitigate p53 function: a mechanism for oncogene-induced genetic instability. *Mol Cell* 2002;9:1031–44.
28. Boyd KE, Farnham PJ. Coexamination of site-specific transcription factor binding and promoter activity in living cells. *Mol Cell Biol* 1999;19:8393–9.
29. Xie S, Lin H, Sun T, Arlinghaus RB. Jak2 is involved in c-Myc induction by Bcr-Abl. *Oncogene* 2002;21:7137–46.
30. Wang X, Cunningham M, Zhang X, Tokarz S, Laraway B, Troxell M, et al. Phosphorylation regulates c-Myc's oncogenic activity in the mammary gland. *Cancer Res* 2011;71:925–36.
31. Hentges P, Ahnesorg P, Pitcher RS, Bruce CK, Kysela B, Green AJ, et al. Evolutionary and functional conservation of the DNA non-homologous end-joining protein, XLF/Cernunnos. *J Biol Chem* 2006;281:37517–26.
32. Hahnel PS, Enders B, Sasca D, Roos WP, Kaina B, Bullinger L, et al. Targeting components of the alternative NHEJ pathway sensitizes KRAS mutant leukemic cells to chemotherapy. *Blood* 2014;123:2355–66.
33. Fattah F, Lee EH, Weisensel N, Wang Y, Lichter N, Hendrickson EA. Ku Regulates the Non-Homologous End Joining Pathway Choice of DNA Double-Strand Break Repair in Human Somatic Cells. *PLoS Genetics* 2010;6(2):e1000855. doi:10.1371/journal.pgen.1000855.
34. Hehlmann R, Jung-Munkwitz S, Saussele S. Treatment of chronic myeloid leukemia when imatinib fails. *Expert Opin Pharmacother* 2011;12:269–83.
35. Jabbour E, Cortes J, Kantarjian H. Long-term outcomes in the second-line treatment of chronic myeloid leukemia: a review of tyrosine kinase inhibitors. *Cancer* 2011;117:897–906.
36. Dang NH, Singla AK, Mackay EM, Jirik FR, Weljie AM. Targeted cancer therapeutics: biosynthetic and energetic pathways characterized by metabolomics and the interplay with key cancer regulatory factors. *Curr Pharm Des* 2014;20:2637–47.
37. Lin CY, Loven J, Rahl PB, Paranal RM, Burge CB, Bradner JE, et al. Transcriptional amplification in tumor cells with elevated c-Myc. *Cell* 2012;151:56–67.
38. Byrne M, Wray J, Reinert B, Wu Y, Nickoloff J, Lee SH, et al. Mechanisms of oncogenic chromosomal translocations. *Ann N Y Acad Sci* 2014;1310:89–97.
39. Fatica A, Fazi F. MicroRNA-regulated pathways in hematological malignancies: how to avoid cells playing out of tune. *Int J Mol Sci* 2013;14:20930–53.
40. O'Donnell KA, Wentzel EA, Zeller KI, Dang CV, Mendell JT. c-Myc-regulated microRNAs modulate E2F1 expression. *Nature* 2005;435:839–43.
41. Sander S, Bullinger L, Klapproth K, Fiedler K, Kestler HA, Barth TF, et al. MYC stimulates EZH2 expression by repression of its negative regulator miR-26a. *Blood* 2008;112:4202–12.
42. Santos FP, Kantarjian HM, Jain N, Manshour T, Thomas DA, Garcia-Manero G, et al. Phase 2 study of CEP-701, an orally available JAK2 inhibitor, in patients with primary or post-polycythemia vera/essential thrombocythemia myelofibrosis. *Blood* 2010;115:1131–6.
43. Arlinghaus RB. The involvement of Bcr in leukemias with the Philadelphia chromosome. *Crit Rev Oncog* 1998;9:1–18.
44. Albajar M, Gomez-Casares MT, Llorca J, Mauleon I, Vaque JP, Acosta JC, et al. MYC in chronic myeloid leukemia: induction of aberrant DNA synthesis and association with poor response to imatinib. *Mol Cancer Res* 2011;9:564–76.
45. Agirre X, Jimenez-Velasco A, San Jose-Eneriz E, Garate L, Bandres E, Cordeu L, et al. Down-regulation of hsa-miR-10a in chronic myeloid leukemia CD34+ cells increases USF2-mediated cell growth. *Mol Cancer Res* 2008;6:1830–40.
46. Xu D, Takeshita F, Hino Y, Fukunaga S, Kudo Y, Tamaki A, et al. miR-22 represses cancer progression by inducing cellular senescence. *J Cell Biol* 2011;193:409–24.
47. Cramer-Morales K, Nieborowska-Skorska M, Scheibner K, Padgett M, Irvine DA, Sliwinski T, et al. Personalized synthetic lethality induced by targeting RAD52 in leukemias identified by gene mutation and expression profile. *Blood* 2013;122:1293–304.
48. Rassool FV, Tomkinson AE. Targeting abnormal DNA double strand break repair in cancer. *Cell Mol Life Sci* 2010;67:3699–710.

Molecular Cancer Research

c-MYC Generates Repair Errors via Increased Transcription of Alternative-NHEJ Factors, LIG3 and PARP1, in Tyrosine Kinase-Activated Leukemias

Nidal Muvarak, Shannon Kelley, Carine Robert, et al.

Mol Cancer Res 2015;13:699-712. Published OnlineFirst March 31, 2015.

Updated version Access the most recent version of this article at:
doi:[10.1158/1541-7786.MCR-14-0422](https://doi.org/10.1158/1541-7786.MCR-14-0422)

Supplementary Material Access the most recent supplemental material at:
<http://mcr.aacrjournals.org/content/suppl/2015/01/09/1541-7786.MCR-14-0422.DC1>

Cited articles This article cites 46 articles, 18 of which you can access for free at:
<http://mcr.aacrjournals.org/content/13/4/699.full#ref-list-1>

Citing articles This article has been cited by 3 HighWire-hosted articles. Access the articles at:
<http://mcr.aacrjournals.org/content/13/4/699.full#related-urls>

E-mail alerts [Sign up to receive free email-alerts](#) related to this article or journal.

Reprints and Subscriptions To order reprints of this article or to subscribe to the journal, contact the AACR Publications Department at pubs@aacr.org.

Permissions To request permission to re-use all or part of this article, use this link
<http://mcr.aacrjournals.org/content/13/4/699>.
Click on "Request Permissions" which will take you to the Copyright Clearance Center's (CCC) Rightslink site.